Journal of Luminescence 134 (2013) 191–194

Contents lists available at SciVerse ScienceDirect

Journal of Luminescence

journal homepage: www.elsevier.com/locate/jlumin

Enhanced orange-red emission by using Mo codoped in Ba_2CaWO_6: Eu^{3+}, Li^+ phosphor under near UV excitation

Xiaoyuan Sun [a,*], Zhendong Hao [b], Chunjie Li [a], Xiaoguang He [a], Haiyan Qi [a], Lijun Yu [a], Yongshi Luo [b], Jiahua Zhang [b], Jiwei Gao [a], Ruixia Zhong [c]

[a] Department of Physics, Changchun Normal University, Changchun 130032, China
[b] Key Laboratory of Excited State Processes, Changchun Institute of Optics, Fine Mechanics and Physics, Chinese Academy of Science, Changchun 130033, China
[c] Department of Materials Science and Engineering, Northeastern University at Qinhuangdao Branch, Qinhuangdao 066004, China

ARTICLE INFO

Article history:
Received 27 November 2011
Received in revised form
20 August 2012
Accepted 27 August 2012
Available online 5 September 2012

Keywords:
Photoluminescence
Phosphor
White light emitting diode

ABSTRACT

The orange-red emitting phosphors $Ba_2Ca_{0.9}Mo_xW_{1-x}O_6$:$Eu^{3+}_{0.05}$, $Li^+_{0.05}$ (x=0, 0.05, 0.1, 0.15, 0.2, 0.25, 0.5, 0.75, and 1.0) and $Ba_2Ca_{1-2y}Mo_{0.2}W_{0.8}O_6$:$Eu^{3+}_y$, Li^+_y (y=0.03, 0.05, 0.07, 0.1, and 0.15) were synthesized. The crystalline structure and photoluminescence properties of these phosphors were described. The strong orange-red emission of Eu^{3+} ($^5D_0$—$^7F_1$ transition) at around 593 nm was observed. Addition of Mo strongly enhances the charge transfer band absorption in the near ultraviolet region that corresponds to near ultraviolet white light emitting diode. The dependence of photoluminescence intensities on Eu^{3+} concentrations with optimal Mo concentration under 400 nm excitation was studied. The phosphor is considered to be a promising orange-red emitting phosphor for near ultraviolet GaN-based white light emitting diode.

1. Introduction

White light emitting diodes (LEDs) are considered the next-generation light source as a consequence of their energy-saving, long lifetime, maintenance and safety [1–5]. In comparison with the commercial white LED fabricated with a blue chip and yellow phosphor YAG:Ce^{3+}, the white LED fabricated with near ultraviolet (UV) chip (400 nm) and corresponding phosphors has higher color stability because all the colors are determined by the phosphors. The near UV chip with excitable phosphors therefore is another attractive combination for white light generation. The essential requirement for phosphor materials is that they should have a high absorption in the near UV spectral region. The search for suitable phosphor is therefore an attractive research task.

In inorganic phosphor, the major emission of Eu^{3+} is attributed to the transition from $^5D_0$ to ^7F_J (J=0, 1, 2, 3, 4), in which the strongest transitions are $^5D_0$—$^7F_1$ and $^5D_0$—$^7F_2$. Both the $^5D_0$— $^7F_1$ and $^5D_0$—$^7F_2$ transitions locate in the orange or red light region [6–9]. Eu^{3+} owns a strong transition of the charge transfer (CT) band, whose site changes according to the host composition; hence the site of the CT band can be controlled by selecting different host materials. Eu^{3+}-doped materials have been widely used in commercial emitting phosphors. Previous investigations have showed that Eu^{3+}-doped tungstates and molybdates exhibited relatively strong absorption in the near UV region and intense orange-red or red emission [10–18]. Eu^{3+}-doped tungstates or molybdates are good candidates as long wave emitting phosphors for the white LEDs applications. It is known that hexavalent Mo and W are stabilized in the ordered double perovskite structure, $A^{II}_2B^{II}B^{VI}O_6$ ($A_2BB'O_6$), in which A^{II} is an alkaline earth ion, B^{II}, a divalent metal ion such as Mg, Ca, Ni, and Cu and B^{VI} a hexavalent Mo or W ion. The Ba_2CaWO_6 compound with Eu^{3+} substituted at the B^{II} site has the high intensity of the $^5D_0$—$^7F_1$ line; however, the CT band lies in the UV region. The MoO_6 octahedra have high absorption in the near UV region, where the near UV LED emission occurs [18]. It is possible to make the solid solution $Ba_2CaMo_xW_{1-x}O_6$ because the ionic radii of tetrahedral Mo^{6+} (0.41 Å) and W^{6+} (0.42 Å) are similar [19]. Hence, we can expect that the progressive replacement of W in Ba_2CaWO_6: Eu^{3+}, Li^+ by Mo leads to changes in the photoluminescence property since the crystal structure influences the luminescence properties. With this in view, a series of orange-red emitting phosphors $Ba_2Ca_{0.9}Mo_xW_{1-x}O_6$:$Eu^{3+}_{0.05}$, $Li^+_{0.05}$ (x=0–1.0) were synthesized by high temperature solid state reaction and its crystalline structure and photoluminescence properties were investigated.

2. Experimental

Polycrystalline powder samples of $Ba_2Ca_{0.9}Mo_xW_{1-x}O_6$:$Eu^{3+}_{0.05}$, $Li^+_{0.05}$ (x=0, 0.05, 0.1, 0.15, 0.2, 0.25, 0.5, 0.75, and 1.0) and $Ba_2Ca_{1-2y}Mo_{0.2}W_{0.8}O_6$:$Eu^{3+}_y$, Li^+_y (y=0.03, 0.05, 0.07, 0.1, and 0.15) phosphors have been synthesized through the high

* Corresponding author. Tel./fax: +86 431 8616 8078.
E-mail address: xueyuan309@yahoo.com.cn (X. Sun).

0022-2313/$ - see front matter © 2012 Elsevier B.V. All rights reserved.
http://dx.doi.org/10.1016/j.jlumin.2012.08.049

temperature solid-state reaction technique. The $BaCO_3$ (99%), $CaCO_3$ (99%), Eu_2O_3 (99.99%), MoO_3 (99.99%), WO_3 (99.98%) and Li_2CO_3 (99.99%) were employed as the raw materials. The Eu^{3+} ions were substituted for the Ca^{2+} site. The charge compensation for the substitution of Ca^{2+} by Eu^{3+} was achieved by adding equimolar concentrations of Li^+. These raw materials in the desired ratio were well milled and heated in air at 600 °C for 6 h in an electric furnace to decompose the carbonates. The obtained products were ground again and heated in air at 850 °C for 5 h, and then reheated at 1250 °C for another 5 h in a muffle furnace. Finally, the samples were ground into powder for characterizations. The final crystalline phase was checked using a Japan Rigaku D/max-rA powder X-ray diffractometer with monochromatized Cu KR radiation (λ=0.15406 Å). The photoluminescence emission (PL) and the photoluminescence excitation (PLE) spectra were measured with a Hitachi F-4500 Spectral spectrophotometer equipped with a xenon lamp. The external quantum efficiency was analyzed with a PL quantum-efficiency measurement system (C9920-02, Hamamatsu Photonics, Shizuoka) under excitation at 400 nm by a 150 W xenon lamp.

3. Results and discussion

3.1. X-ray diffraction analysis

The X-ray diffraction patterns of the $Ba_2Ca_{0.9}Mo_xW_{1-x}O_6$:$Eu^{3+}_{0.05}$, $Li^+_{0.05}$ (x=0, 0.1, 0.25, 0.5, 0.75, and 1.0), Ba_2CaWO_6, and Ba_2CaMoO_6 phosphors are shown as in Fig. 1. It is exhibited that Ba_2CaWO_6 presents a single phase formation that belongs to the space group $Fm\bar{3}m$, Z=4 (JCPDS card no. 22-0509). Ba_2CaMoO_6 crystallizes in the pseudo cubic structure with space group $Fm\bar{3}m$ also. It is isostructural with the tungstate analogues [20]. No impurity line was found in the X-ray diffraction patterns of the $Ba_2Ca_{0.9}Mo_xW_{1-x}O_6$:$Eu^{3+}_{0.05}$, $Li^+_{0.05}$ (x=0, 0.1, 0.25, 0.5, 0.75, and 1.0) phosphors clearly indicating that the compounds formed are single phase and Eu^{3+} incorporation has been achieved. When Mo is added into $Ba_2Ca_{0.9}WO_6$:$Eu^{3+}_{0.05}$, $Li^+_{0.05}$ phosphors, the samples are still single phase with good crystalline nature, indicating that the samples formed solid solutions.

3.2. PLE and PL spectra

The PLE spectra of $Ba_2Ca_{0.9}Mo_xW_{1-x}O_6$:$Eu^{3+}_{0.05}$, $Li^+_{0.05}$ (x=0, 0.05, 0.1, 0.2, 0.25, 0.5, 0.75, and 1.0) phosphors, monitoring the 593 nm Eu^{3+} emission ($^5D_0$—$^7F_1$), are presented in Fig. 2. The PLE spectra of the Eu^{3+} ion consist of a broad band, which is due to a CT band of the tungstate and molybdate framework. Additional peaks are observed at 466 nm ($^7F_0$—$^5D_2$) and 528 nm ($^7F_0$—$^5D_1$), which are due to f—f electronic transitions of Eu^{3+} ion. The intensity of the CT band is very high compared to that of the f—f transitions of Eu^{3+} ion. The CT band of $Ba_2Ca_{0.9}WO_6$:$Eu^{3+}_{0.05}$, $Li^+_{0.05}$ phosphor for the $^5D_0$—$^7F_1$ emission of Eu^{3+} ion exhibits a broad band centered at about 300 nm, and that of $Ba_2Ca_{0.9}MoO_6$:$Eu^{3+}_{0.05}$, $Li^+_{0.05}$ phosphor centered around 400 nm. As Mo concentration increases, the CT intensity of $Ba_2Ca_{0.9}WO_6$:$Eu^{3+}_{0.05}$, $Li^+_{0.05}$ phosphor decrease. The CT bands shift to the longer wavelength side with increasing Mo concentrations from 0 to 1. The width of CT bands reach their maximum at around x=0.2. The photoluminescence property of $Ba_2Ca_{0.9}MoO_6$:$Eu^{3+}_{0.05}$, $Li^+_{0.05}$ phosphor was reported as a potential orange-red emitting phosphor for white LEDs based on near UV GaN-based LEDs. Intense orange-red emission was observed in the case of $Ba_2Ca_{0.9}MoO_6$:$Eu^{3+}_{0.05}$, $Li^+_{0.05}$ phosphor [18]. In our research paper, the excitation intensities of $Ba_2Ca_{0.9}Mo_xW_{1-x}O_6$:$Eu^{3+}_{0.05}$, $Li^+_{0.05}$ (x=0.1, 0.2, 0.25, 0.5, and 0.75) are stronger than that of $Ba_2Ca_{0.9}MoO_6$:$Eu^{3+}_{0.05}$, $Li^+_{0.05}$ phosphor in the near UV region, as shown in Fig. 2. As Mo is incorporated into the matrix of the $Ba_2Ca_{0.9}WO_6$: $Eu^{3+}_{0.05}$, $Li^+_{0.05}$ phosphor, especially for the concentration x=0.2, the excitation intensities of the near UV region are greatly enhanced.

The PL spectra of $Ba_2Ca_{0.9}WO_6$:$Eu^{3+}_{0.05}$, $Li^+_{0.05}$, $Ba_2Ca_{0.9}Mo_{0.2}W_{0.8}O_6$:$Eu^{3+}_{0.05}$, $Li^+_{0.05}$, and $Ba_2Ca_{0.9}MoO_6$:$Eu^{3+}_{0.05}$, $Li^+_{0.05}$ phosphors under 400 nm excitation wavelength are presented in Fig. 3. The PL spectra of $Ba_2Ca_{0.9}WO_6$:$Eu^{3+}_{0.05}$, $Li^+_{0.05}$, $Ba_2CaMo_{0.2}W_{0.8}O_6$:$Eu^{3+}_{0.05}$, $Li^+_{0.05}$, and $Ba_2Ca_{0.9}MoO_6$:$Eu^{3+}_{0.05}$, $Li^+_{0.05}$ phosphor show a strong emission line at 593 nm, which arise from the $^5D_0$—$^7F_1$ transitions of Eu^{3+} ion [21]. The PL spectra of $Ba_2Ca_{0.9}Mo_{0.2}W_{0.8}O_6$:$Eu^{3+}_{0.05}$, $Li^+_{0.05}$ phosphor show the other two peaks at around 581 nm and 611 nm, which arise from the $^5D_0$—$^7F_0$ and the $^5D_0$—$^7F_2$ transitions of Eu^{3+}, respectively. The emission at 593 nm is due to the $^5D_0$—$^7F_1$ magnetic dipole transition, which is insensitive to the site symmetry. The emission at 611 nm is due to the $^5D_0$—$^7F_2$ electric dipole transition, induced by the lack of inversion symmetry at the Eu^{3+} site [21]. The emission intensity ratio of the $^5D_0$—$^7F_2$ to $^5D_0$—$^7F_1$ transitions strongly depend on the local symmetry of the Eu^{3+} ions in host lattice. When the Eu^{3+} ions occupy symmetric sites, the ratio is smaller. The emission spectrum of the $Ba_2Ca_{0.9}Mo_{0.2}W_{0.8}O_6$:$Eu^{3+}_{0.05}$, $Li^+_{0.05}$ phosphor exhibits weak emission ascribed to the $^5D_0$—$^7F_2$ transition at

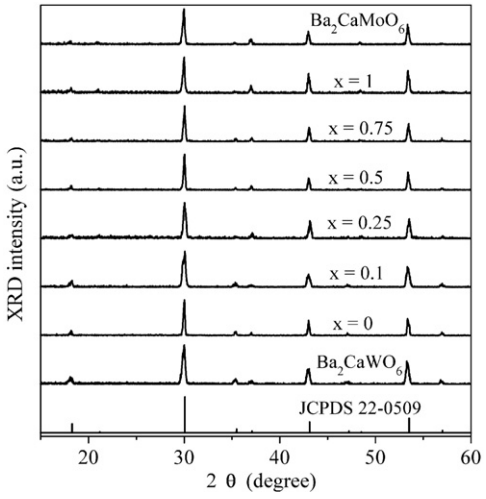

Fig. 1. X-ray diffraction patterns of the $Ba_2Ca_{0.9}Mo_xW_{1-x}O_6$:$Eu^{3+}_{0.05}$, $Li^+_{0.05}$ (x=0.05, 0.1, 0.25, 0.5, 0.75, and 1.0), Ba_2CaWO_6, and Ba_2CaMoO_6 phosphors.

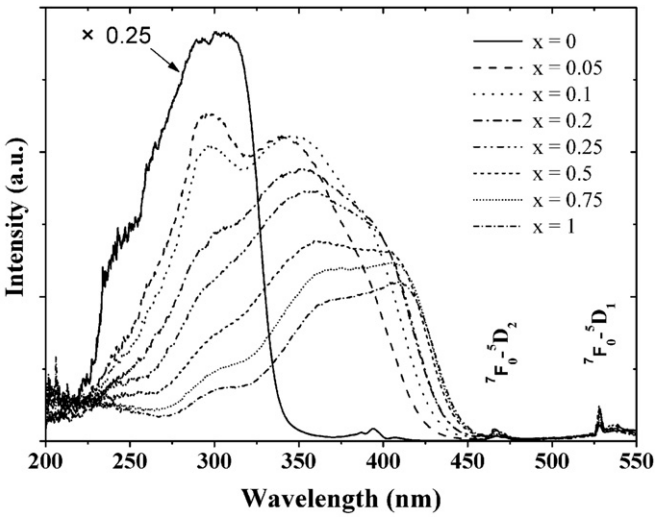

Fig. 2. The PLE spectra (λem=593 nm) of $Ba_2Ca_{0.9}Mo_xW_{1-x}O_6$:$Eu^{3+}_{0.05}$, $Li^+_{0.05}$ (x=0, 0.05, 0.1, 0.2, 0.25, 0.5, 0.75, and 1.0).

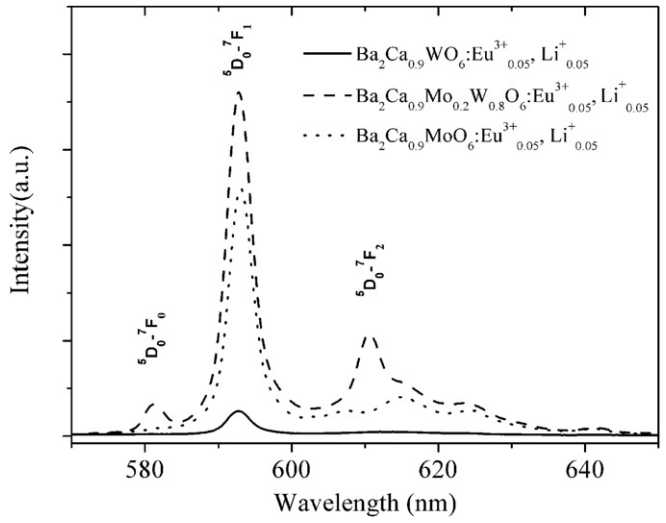

Fig. 3. The PL spectra (λex=400 nm) of $Ba_2Ca_{0.9}WO_6:Eu^{3+}_{0.05}$, $Li^{+}_{0.05}$, $Ba_2Ca_{0.9}Mo_{0.2}W_{0.8}O_6:Eu^{3+}_{0.05}$, $Li^{+}_{0.05}$, and $Ba_2Ca_{0.9}MoO_6:Eu^{3+}_{0.05}$, $Li^{+}_{0.05}$.

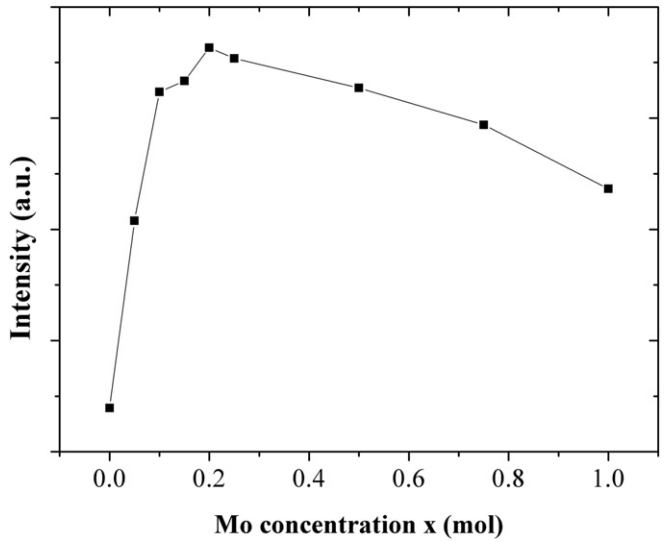

Fig. 4. The dependence of the Eu^{3+} emission intensities on Mo concentration in $Ba_2Ca_{0.9}Mo_xW_{1-x}O_6:Eu^{3+}_{0.05}$, $Li^{+}_{0.05}$ under 400 nm excitation.

611 nm and strong emission ascribed to the $^5D_0$—$^7F_1$ at 593 nm, thus indicating that the Eu^{3+} ion is located at an almost symmetric position in the matrix. This is so because the compound has pseudo cubic structure and the Mo–O–Eu (B–O–B′) angle is close to 180°. This makes the energy transfer from the host to Eu^{3+} very efficient and the energy transfer could be due to exchange interactions.

The $^5D_0$—$^7F_1$ transitions are greatly enhanced when Mo is incorporated as shown in Fig. 3. Therefore, when Mo is substituted for W ions the Eu^{3+} PL intensity is greatly enhanced. With the purpose of the phosphor application for white LEDs with near UV (around 400 nm) GaN-based chips as excitation sources, the intensity of the PL spectra at around 400 nm are compared to each other. Fig. 4 depicts the dependence of the Eu^{3+} emission intensities on the Mo concentration in $Ba_2Ca_{0.9}Mo_xW_{1-x}O_6:Eu^{3+}_{0.05}$, $Li^{+}_{0.05}$ phosphors under 400 nm excitation. The Eu^{3+} emission intensities initially increase with increasing Mo concentration, reach a maximum around x=0.2, then decrease.

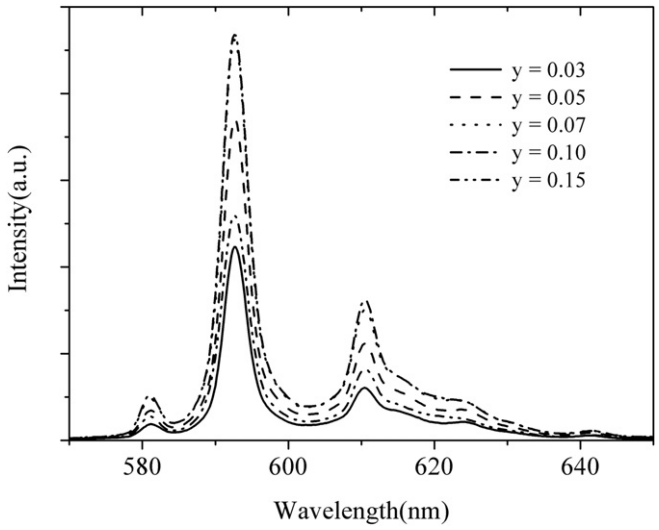

Fig. 5. The PL spectra of $Ba_2Ca_{1-2y}Mo_{0.2}W_{0.8}O_6:Eu^{3+}_y$, Li^{+}_y with different Eu^{3+} concentrations (y=0.03, 0.05, 0.07, 0.1, and 0.15) under 400 nm excitation.

Table 1
Quantum efficiency of $Ba_2Ca_{1-2y}Mo_xW_{1-x}O_6:Eu^{3+}_y$, Li^{+}_y phosphors.

(x, y)	(0, 0.05)	(0.1, 0.05)	(0.2, 0.05)	(0.5, 0.05)	(1, 0.05)
η (%)	2.3	6.1	5.7	4.9	2.9
(x, y)	(0.2, 0.03)	(0.2, 0.05)	(0.2, 0.07)	(0.2, 0.1)	(0.2, 0.15)
η (%)	3.6	5.7	6.7	7.7	5.2

3.3. Dependence of PL intensities on Eu^{3+} concentrations

Fig. 5 illustrates the PL spectra of $Ba_2Ca_{1-2y}Mo_{0.2}W_{0.8}O_6:Eu^{3+}_y$, Li^{+}_y presenting different Eu^{3+} concentrations (y=0.03, 0.05, 0.07, 0.1, and 0.15) with optimal Mo concentration at around 0.2 under 400 nm excitation. The emission intensities initially increase with increasing Eu^{3+} ion concentration and reach a maximum at around 0.1. Therefore, the most efficient concentrations for the maximum orange-red emission occur at 0.1 and 0.2 for Eu^{3+} and Mo, respectively.

3.4. Quantum efficiency of $Ba_2Ca_{1-2y}Mo_xW_{1-x}O_6:Eu^{3+}_y$, Li^{+}_y phosphors

The external quantum efficiency of $Ba_2Ca_{1-2y}Mo_xW_{1-x}O_6:Eu^{3+}_y$, Li^{+}_y phosphors are listed in Table 1. The quantum efficiency values of $Ba_2Ca_{0.9}WO_6:Eu^{3+}_{0.05}$, $Li^{+}_{0.05}$ (η=2.3%) and $Ba_2Ca_{0.9}MoO_6:Eu^{3+}_{0.05}$, $Li^{+}_{0.05}$ (η=2.9%) are lower than that of the solid solution $Ba_2Ca_{0.9}Mo_xW_{1-x}O_6:Eu^{3+}_{0.05}$, $Li^{+}_{0.05}$ (x=0.1, 0.2, 0.25, 0.5, 0.75, η=4.9%–6.1%). As Mo is incorporated into the matrix of the $Ba_2Ca_{0.9}WO_6:Eu^{3+}_{0.05}$, $Li^{+}_{0.05}$ phosphor, the quantum efficiency is improved. For the Mo concentration x=0.2 in $Ba_2Ca_{1-2y}Mo_xW_{1-x}O_6:Eu^{3+}_y$, Li^{+}_y, the quantum efficiency of the samples approaches a maximum at y=0.1. The maximum quantum efficiency is 7.7%.

4. Conclusions

In conclusion, a series of orange-red phosphors of $Ba_2Ca_{0.9}Mo_xW_{1-x}O_6:Eu^{3+}_{0.05}$, $Li^{+}_{0.05}$ (x=0–1.0) and $Ba_2Ca_{1-2y}Mo_{0.2}W_{0.8}O_6:Eu^{3+}_y$, Li^{+}_y (y=0.03, 0.05, 0.07, 0.1, and 0.15) have been synthesized and the luminescence properties of Eu^{3+} were presented. Addition of Mo strongly enhances the orange-red emission of Eu^{3+} ($^5D_0$—$^7F_1$) in $Ba_2Ca_{0.9}WO_6:Eu^{3+}_{0.05}$, $Li^{+}_{0.05}$ phosphor under excitations of

400 nm that correspond to near UV LED. The higher molybdenum content shifts the PLE spectra maximum from UV to near UV region, where the LED emission occurs. The most efficient concentrations for the maximum orange-red emission occur at 0.1 and 0.2 for Eu^{3+} and Mo, respectively. Moreover, the higher quantum efficiency was also obtained at these concentrations. The phosphor is considered to be a promising orange-red emitting phosphor for near UV GaN-based white LED.

Acknowledgments

This work is financially supported by the Technology Development Plan of Jilin Province (Grant n o.201101106), the Major Research Plan of the Natural Science Foundation of Hebei Province, China (Grant no. A2010001379), and the Natural Science Foundation of Changchun Normal University.

References

[1] M.Y. Wang, J.H. Zhang, X. Zhang, Y.S. Luo, X.G. Ren, S.Z. Lu, X.R. Liu, X.J. Wang, J. Phys. D Appl. Phys. 41 (2008) 205103.
[2] R.J. Xie, N. Hirosaki, K. Sakuma, Y. Yamamoto, M. Mitomo, Appl. Phys. Lett. 84 (2004) 5404.
[3] S.X. Yan, J.H. Zhang, X. Zhang, S.Z. Lu, X.G. Ren, Z.G. Nie, X.J. Wang, J. Phys. Chem. C 111 (2007) 13256.
[4] H.S. Jang, D.Y. Jeon, Appl. Phys. Lett. 90 (2007) 041906-1.
[5] N. Hirosaki, R.J. Xie, K. Kimoto, T. Sekiguchi, Y. Yamamoto, T. Suehiro, M. Mitomo, Appl. Phys. Lett. 86 (2005) 211905-1.
[6] F. You, S. Huang, S. Liu, Y. Tao, J. Lumin. 110 (2004) 95.
[7] M. Kottaisamy, R. Jagannathan, Ravi P. Rao, M. Avudaithai, L.K. Srinivasan, V. Sundaram, J. Electrochem. Soc. 142 (1995) 3205.
[8] Y. Tian, B.J. Chen, R.N. Hua, J.S. Sun, L.H. Cheng, H.Y. Zhong, X.P. Li, J.S. Zhang, Y.F. Zheng, T.T. Yu, L.B. Huang, H.Y. Yu, J. Appl. Phys. 109 (2011) 053511-1.
[9] F. Lei, B. Yan, H.H. Chen, J.T. Zhao, J. Am. Ceram. Soc. 92 (6) (2009) 1262.
[10] Y.S. Hu, W.D. Zhuang, H.Q. Ye, D.H. Wang, S.S. Zhang, X.W. Huang, J. Alloys. Compd. 390 (2005) 226.
[11] J.S. Kim, P.E. Jeon, Y.H. Park, J.C. Choi, H.L. Park, Appl. Phys. Lett. 85 (17) (2004) 3696.
[12] J.S. Kim, P.E. Jeon, J.C. Choi, H.L. Park, Appl. Phys. Lett. 84 (15) (2004) 2931.
[13] S. Neeraj, N. Kijima, A.K. Cheetham, Chem. Phys. Lett. 387 (2004) 2.
[14] V. Sivakumar, U.V. Varadaraju, J. Electrochem. Soc. 154 (1) (2007) J28.
[15] G.H. Lee, S. Kang, J. Lumin. 131 (2011) 2582.
[16] F. Lei, B. Yan, H.H. Chen, J. Solid State Chem. 181 (2008) 2845.
[17] F.Y. Yu, J. Zuo, Z. Zhao, C.Y. Jiang, Q. Yang, Mater. Res. Bull. 46 (2011) 1327.
[18] V. Sivakumar, U.V. Varadaraju, Electrochem. Solid State Lett. 9 (6) (2006) H35.
[19] R.D. Shannon, Acta Crystallogr. Sect. A: Cryst. Phys. Diffr. Theor. Gen. Crystallogr. A32 (1976) 751.
[20] E.G. Steward, H.P. Rooksby, Acta Cryst. 4 (1951) 503.
[21] S. Shionoya, W.M. Yen, Phosphor Handbook (1999) 204.